NUCLEAR SCIENCE AND ENGINEERING: 35, 91-103 (1969)

The Neutron Spectrum from a Fission Source in Graphite

A. E. Profio, H M. Antúnez,* and D. L Huffman

Gulf General Atomic Incorporated, P.O. Box 608, San Diego, California 92112

Received June 20, 1968
Revised August 23, 1968

Time-of-flight measurements of the neutron angular flux spectrum in graphite have been made to provide a standard of comparison for neutron penetration calculations. The spectrum from 0.002 eV to 15 MeV was measured with an accuracy of ±13 to 32% and a resolution of ±2 to 10%, at angles from 0 to 60° and penetrations to 66 cm. Comparisons with Monte Carlo and discrete ordinates calculations using ENDF/B cross sections indicate fairly good agreement except in resonances and near zero degrees for discrete ordinates. Scalar fluxes have also been calculated with the moments method.

I. INTRODUCTION

Given the nuclear data, modern codes and computers make possible a theoretically rigorous solution of neutron transport. Nevertheless, practical considerations in storage, running time, and preparation of data lead to approximations in the coding and input that need to be tested against experiment. In multigroup discrete-ordinates codes, for example, the continuous energy-angle-spatial distributions of the flux and nuclear data are approximated by discrete energy groups, angular quadrature, truncation of the scattering kernel, and finite spatial mesh. Furthermore, the solution is iterative and convergence is not assured. In Monte Carlo, practical requirements in running times for acceptable statistical precision require biasing. However, the biasing may give not only an inaccurate mean but also an inaccurate, often optimistic, estimate of the variance. Mistakes in programming, which are hard to detect in these complicated codes, may also exist. We have measured the neutron angular flux spectrum from a fission source in graphite[1] by the pulsed-source, time-of-flight method to provide a more differential test than has been possible up to now. Recently, Coates *et al.*[2] published similar measurements, but over a more limited range of energy, angle, and depth of penetration.

Comparisons of measurements with calculations also provide a test of the nuclear data, and of the way in which the data are averaged or otherwise handled, in a configuration which can be chosen to approximate that in an actual application. Thus, the sensitivity of the calculation to nuclear data can be judged. Measurements of the spectrum and angular distributions are particularly useful since one can often detect specific energy ranges where the data are or are not adequate. Furthermore, the angular flux spectrum vs position provides all the information needed to compute integral quantities, such as reaction rates, heating, dose in tissue, radiation damage in materials, etc. In this experiment, we chose graphite as a common nonhydrogenous reactor and shielding material with reasonably well-known cross sections. However, even in graphite, we found a discrepancy that may be due to an error in the total cross section.

The geometry was simple, approximating a point isotropic fission source in an infinite medium. The spectrum and other characteristics of the source were measured to avoid any ambiguity

*Permanent address: Centro Atomico, Bariloche, Argentina.

[1]A. E. PROFIO, H. M. ANTUNEZ, and T. G. WILLIAMSON, "Measurements of the Neutron Angular Flux Spectrum in Graphite," DASA-1933, General Dynamics Corporation, General Atomic Division (1966).

[2]M. S. COATES, D. B. GAYTHER, and P. D. GOODE, "Measurements of Fast Neutron Spectra in Reactor Materials," AERE-R5364, United Kingdom Atomic Energy Research Establishment (1968).

in this regard. Since this is the first complete publication of our results, we have gone into some detail on the experimental method used.

The measurements have been compared with angular flux spectrum calculations performed with the 05R Monte Carlo code and the 1DF version of the DTF-IV discrete ordinates code. In addition, scalar flux spectrum calculations are available from the NBS moments code. In general, agreement is fairly good, but discrepancies were found at zero degrees and in the 3.5-MeV resonance.

II. EXPERIMENTAL PROCEDURE

In the time-of-flight method, the neutron energy and angular distribution are measured by extracting a collimated beam from the experimental assembly at the desired position and angle and measuring the time of flight over a fixed, known distance (50 m in this experiment). The experimental layout is illustrated schematically in Fig. 1. Time zero is defined by pulsing the neutron source. The source in our experiment was a small water-cooled, spherical, depleted uranium target[3] irradiated by a pulsed 28-MeV electron beam from the linear accelerator. The electrons generate bremsstrahlung, which in turn produces a broad, fission-type spectrum of fast neutrons by the (γ,n) and (γ,F) reactions. Neutron emission is coincident with, and proportional to, the electron current pulse, and the length of the current pulse is made small compared to the flight time of the fastest neutron detected. In a shield placed around the target, there is an additional delay and variance in emission because of the time for a source neutron to slow down and diffuse to the point where it enters the collimated beam to the detector. A small correction is made for the mean emission time, but the variance of emission time in graphite ultimately limits the energy resolution. Nevertheless, resolutions of 10% to better than 2% are achieved over most of the energy range from 15 MeV to 0.002 eV (the poorest resolution, 35%, occurs near 0.1 eV). This is considerably better than is available with other methods.

The flight path consists essentially of a precollimator, collimators at 16 m and 32 m, a shielded detector at 50 m, and large-diameter steel drift tubes evacuated to rough vacuum. The precollimator and the drift tube to 16 m are located in the wall of a concrete- and earth-shielded experimental cell. The precollimator consists of steel tubing filled with a lead–boric-acid–epoxy mixture. The collimators are made of hydrated boric acid backed by lead or borated paraffin wax covered in cadmium (for thermal-neutron measurements). Mylar or aluminum windows on the drift tubes permit the collimators and detector, as well as the experimental assembly, to be located in air. Tests have shown that stray background with this system is less than ambient

[3] A. E. PROFIO, M. R. HACKNEY, G. D. TRIMBLE, H. M. ANTUNEZ, and J. L. RUSSELL, Jr., "Angular Flux Spectrum and Other Characteristics of the 7.62-cm Diameter Uranium Target," GA-7409, General Atomic (1966).

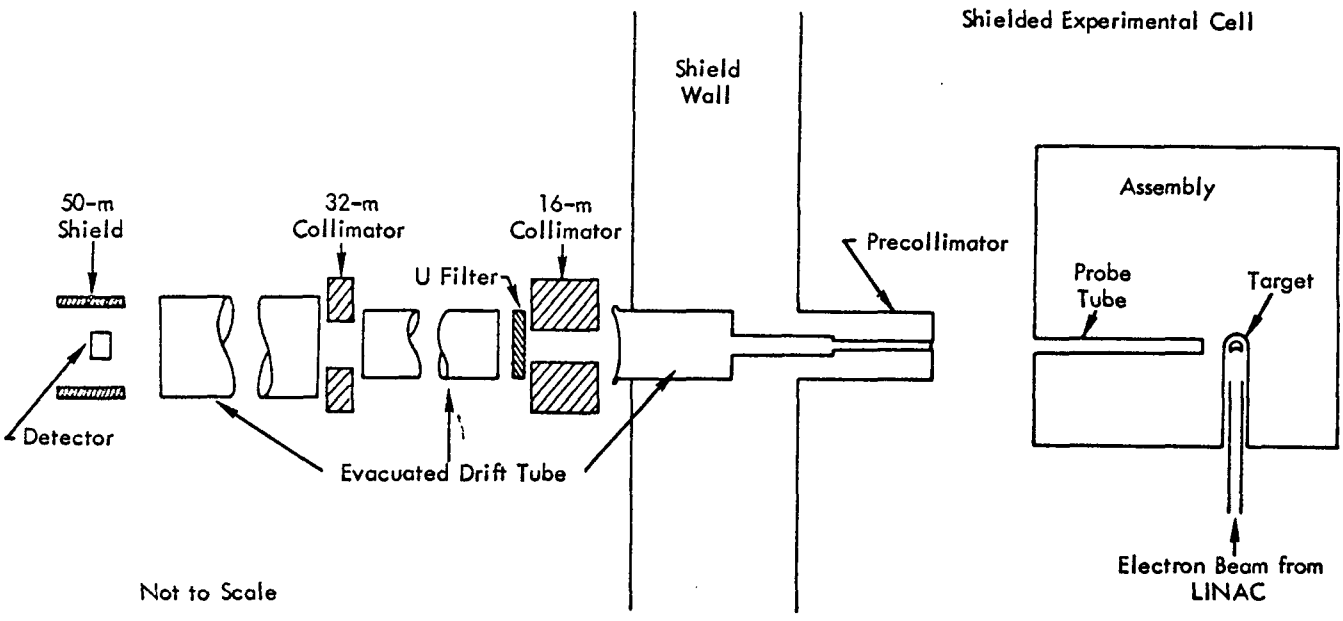

Fig. 1. Schematic experimental layout.

radioactivity. Certain fast and intermediate spectrum measurements were made with a 3.144-cm-thick depleted uranium filter in the flight path at 16 m to attenuate the bremsstrahlung and beam-associated gamma rays. All measurements with the intermediate energy detector incorporated a ^{10}B filter in the flight path, to eliminate overlap of thermal neutrons from preceding pulses.

The neutrons from 0.8- to 15-MeV energy were detected in either a 5.08-cm-diam × 5.08-cm-high NE211 scintillator (Nuclear Enterprises, Ltd.), or a 12.7-cm-diam × 12.7-cm-thick NE213 scintillator.[4] A boron capture detector[5] was used from 200 eV to 0.8 MeV. This detector consisted of a 19.0-cm-diam disk of borated paraffin backed by a nonhydrogenous scintillator (NE226) to detect the 478-keV boron capture gamma ray. Neutrons with energies below 200 eV were detected in a 91-cm-diam bank of enriched BF_3 counters.

After correcting for dead time in the analyzer, subtracting background, and converting to counts per unit energy, $C(E)$, the angular flux per monitor count is calculated as follows:

$$\psi(E) = \frac{C(E)}{G(E)\ T(E)\ (A_d/L^2)\ \eta A_s\ M} \quad , \qquad (1)$$

where

$G(E)$ = intrinsic efficiency, counts/neutron incident

$T(E)$ = flight path transmission

A_d = detector area, cm^2

L = flight distance, cm

A_d/L^2 = solid angle, steradian

ηA_s = efficiency of the collimation system times the reference viewed area perpendicular to the beam, cm^2

M = monitor count (or relative fluence at the monitor).

The collimation efficiency is defined as the counting rate with the collimators in place, divided by the counting rate without collimators. It is calculated by a ray-tracing code, CAP[6] and accounts for the angular transmission of the collimators.

All measurements are normalized to an arbitrary standard source intensity by activation of monitor foils in a reproducible geometry. The graphite measurements were normalized to the fluence recorded by activation of a sulfur pellet, 3.81 cm in diameter × 0.95 cm thick, located ~19 cm from the center of the target. The beta activity from the $^{32}S(n,p)^{32}P$ reaction (effective threshold, 3 MeV) was counted.

Two graphite assemblies were studied. The fast- and intermediate-spectrum measurements were made in the stack of reactor-grade graphite bars depicted schematically in Fig. 2. The bars were accurately machined and joints were staggered in more than the one direction shown, to avoid any streaming. The overall dimensions were 132 cm wide × 152 cm long × 152 cm high, and the target was located in a 8.9-cm-diam cavity in the vertical midplane, 56 cm from the bottom and 56 cm from the right face. The target was designed for spherically symmetric emission, and the dimensions of the graphite were chosen to permit analysis as an infinite medium. The neutron beam was extracted by opening a 7.62-cm-diam probe hole to the proper depth and angle and elevating the stack to align the hole on the collimator.

Measurements below 200 eV were made in a smaller stack, 112 cm wide × 112 cm high × 132 cm long. The target was located on the long axis, 56 cm from one end. Measurements (at 0 or 90° to the long axis) were made in the horizontal midplane, with the stack oriented and translated

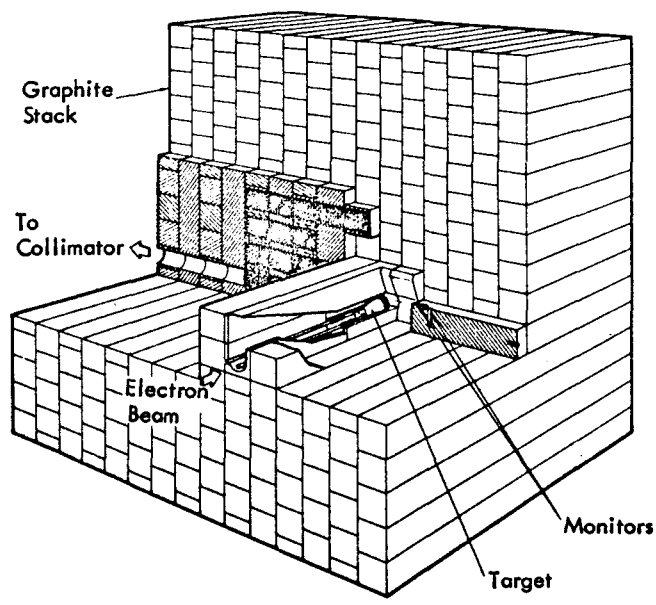

Fig. 2. Graphite stack for fast spectrum measurements.

[4]A. E. PROFIO, P. L. PHELPS, J. W. RIGGS, and J. C. YOUNG, "Design and Efficiency Calibration of the 5-cm and 13-cm Fast Neutron Detectors," GA-7483, General Atomic (1966).

[5]A. E. PROFIO, "The Boron Capture Detector for Time-of-Flight Measurements," GA-7578, General Atomic (1966).

[6]H. C. HONECK, "CAP, A Collimator Analysis Program," GA-5418, General Dynamics Corporation, General Atomic Division (1964).

relative to the collimator as required. Neutrons were extracted from a 3.81-cm-diam probe hole. The smaller stack was designed for a faster dieaway of the thermal-neutron flux and for symmetrical target placement to aid the analysis. Neither it nor the larger assembly was effectively infinite for thermal neutrons, and leakage must be taken into account in the thermal flux calculation. The stack was covered with 0.32 cm of borated polyethylene and 0.051 cm of cadmium to establish the thermal-neutron boundary condition.

The nuclear density of carbon was 0.0833 ($\pm 0.6\%$) nuclei $(b\ cm)^{-1}$, and the nominal temperature was 298°K. A spectroscopic analysis showed impurities were negligible in fast-neutron penetration. A thermal-neutron absorption cross section of 5.31 mb (0.0253 eV) was derived from pulsed-source, flux dieaway measurements.

The target consisted of a 7.62-cm-diam sphere of depleted uranium (0.22 wt% ^{235}U) plated with 0.0254 cm of copper and 0.0127 cm of nickel and surrounded by a layer of water 0.20 ± 0.03 cm thick and a type 304 stainless steel jacket, 0.07 cm thick. A reentrant hole, 2.54 cm in diameter, admitted the electron beam to within 0.85 cm of the sphere. This hole is also lined with a water jacket. However, for most purposes, spherical symmetry can be assumed in calculations. The measured neutron emission is spherically symmetric to within ± 5%. Measurements of the spatial distribution of photofission products suggest generating the neutrons uniformly in a spherical volume with a radius of 0.85 cm, and isotropic emission may be assumed. Alternatively, the outward-directed energy-angle distribution at the target surface may be generated, and the uranium, water, and stainless steel are included only to account for interactions with backscattered neutrons. The hemisphere-integrated leakage spectrum, measured by the time-of-flight method with a large collimator, is plotted in Fig. 3 and listed in Table I (normalized to one neutron between 0.22

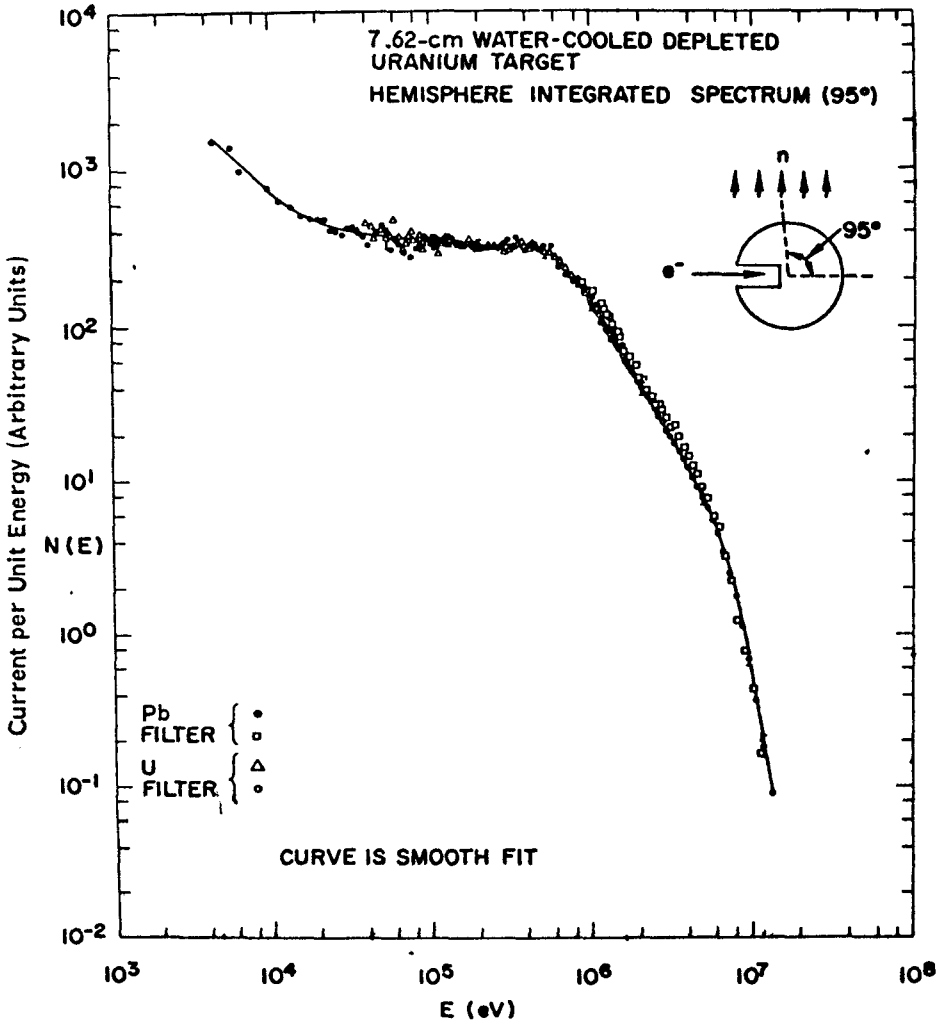

Fig. 3. Target leakage spectrum.

TABLE I

Normalized Target Leakage Spectrum

Energy (eV)	$N(E)$	Energy (eV)	$N(E)$
2.2800 + 05	9.3922 - 07	1.4300 + 06	2.2159 - 07
2.3900 + 05	8.8415 - 07	1.4800 + 06	2.0672 - 07
2.5100 + 05	9.2784 - 07	1.5500 + 06	1.9265 - 07
2.6400 + 05	8.8965 - 07	1.6100 + 06	1.8116 - 07
2.7800 + 05	9.0287 - 07	1.6800 + 06	1.6438 - 07
2.9400 + 05	8.4926 - 07	1.7600 + 06	1.5583 - 07
3.1000 + 05	8.6542 - 07	1.8400 + 06	1.4496 - 07
3.2800 + 05	8.9883 - 07	1.9200 + 06	1.3060 - 07
3.4800 + 05	9.3518 - 07	2.0100 + 06	1.2216 - 07
3.6900 + 05	9.6676 - 07	2.1100 + 06	1.1287 - 07
3.9200 + 05	8.7166 - 07	2.2200 + 06	1.0589 - 07
4.1800 + 05	9.1609 - 07	2.3300 + 06	9.7190 - 08
4.4700 + 05	9.1462 - 07	2.4500 + 06	8.8121 - 08
5.1300 + 05	8.4449 - 07	2.5800 + 06	7.9492 - 08
5.5200 + 05	8.4412 - 07	2.7300 + 06	7.4866 - 08
5.9500 + 05	7.8868 - 07	2.8800 + 06	6.4034 - 08
6.4300 + 05	7.4499 - 07	3.0500 + 06	5.9922 - 08
6.9800 + 05	6.7266 - 07	3.2300 + 06	5.2762 - 08
7.6000 + 05	6.0840 - 07	3.4400 + 06	4.7438 - 08
7.7600 + 05	6.9065 - 07	3.6600 + 06	4.1711 - 08
7.9900 + 05	6.2970 - 07	3.9000 + 06	3.7708 - 08
8.2300 + 05	6.0179 - 07	4.1700 + 06	3.2373 - 08
8.7500 + 05	5.3166 - 07	4.4600 + 06	2.7960 - 08
9.0300 + 05	5.0926 - 07	4.7900 + 06	2.4145 - 08
9.3200 + 05	4.6667 - 07	5.1600 + 06	2.0418 - 08
9.6200 + 05	4.3767 - 07	5.5700 + 06	1.7128 - 08
9.9400 + 05	4.0022 - 07	6.0300 + 06	1.4151 - 08
1.0300 + 06	3.8773 - 07	6.5600 + 06	1.0589 - 08
1.0600 + 06	3.6298 - 07	7.1500 + 06	7.7620 - 09
1.1000 + 06	3.4389 - 07	7.8300 + 06	5.5002 - 09
1.1400 + 06	3.2553 - 07	8.6000 + 06	3.4433 - 09
1.1800 + 06	3.0435 - 07	9.5000 + 06	2.1226 - 09
1.2200 + 06	2.8540 - 07	1.0550 + 07	1.1408 - 09
1.2700 + 06	2.6264 - 07	1.1790 + 07	5.7095 - 10
1.3200 + 06	2.4446 - 07	1.3250 + 07	2.7828 - 10
1.3700 + 06	2.3201 - 07	1.5520 + 07	1.0453 - 10

and 15 MeV). The angular distribution at the target surface is given by groups in Table II as a cumulative probability vs μ, the cosine of the angle between the radius vector and the direction of the neutron. Beam conditions were typically 0.02-μsec burst width at 360 pulses/sec for the fast-neutron spectrum measurements, 0.1 μsec at 180 pulses/sec for the intermediate spectrum measurements, and 0.5 to 4.5 μsec at 7.5 pulses/sec for the thermal spectrum measurements. Further details on the method may be found in Ref. 7.

III. RESULTS AND ERROR ANALYSIS

The time-of-flight spectrum measurements are summarized in Table III. The spectra are plotted in Figs. 4 through 9. Tabulated results may be found in Ref. 1.

The energy scale, which depends on the flight distance, zero time determination, and mean emission time, is known to better than 1%. The energy resolution is a function of the timing uncertainties due to the neutron burst width, detector response, variance in emission time, zero channel error, and channel width. The fast-neutron detectors have a timing jitter of $\sim$0.01 μsec; the boron capture detector timing precision is $\sim$0.05 μsec, and that of the BF_3 detector is $\sim$1 μsec. The variance in emission time is negligible compared to other uncertainties above 1 eV, but results in a 35% energy resolution near 0.1 eV and 12% near 0.01 eV. The zero channel error of $\pm$ 0.015 μsec

[7] J. L. RUSSELL et al., "Determination of Neutron Spectra in Bulk Media by Time-of-Flight," *Pulsed Neutron Research*, Vol. II, p. 445, International Atomic Energy Agency, Vienna (1965).

TABLE II

Cumulative Probability for Source Angular Distribution

E(MeV)	1.00-0.99	0.99-0.875	0.875-0.750	0.750-0.625	0.625-0.500	0.500-0.375	0.375-0.250	0.250-0.125	0.125-0.0
15.00 -10.00	0.37515	0.94507	0.98778	0.99932	1.00000	1.00000	1.00000	1.00000	1.00000
10.00 - 6.70	0.33407	0.86961	0.92311	0.94178	0.99883	1.00000	1.00000	1.00000	1.00000
6.70 - 4.49	0.31717	0.87134	0.94723	0.97849	0.99208	0.99749	0.99952	1.00000	1.00000
4.49 - 3.01	0.29114	0.82415	0.91232	0.95396	0.97613	0.98740	0.99332	0.99762	1.00000
3.01 - 2.02	0.28429	0.80479	0.89597	0.94233	0.96924	0.98280	0.98957	0.99694	1.00000
2.02 - 1.35	0.26970	0.77257	0.87008	0.92375	0.95728	0.97561	0.98558	0.99449	1.00000
1.35 - 0.821	0.22590	0.69746	0.81994	0.89410	0.94317	0.97010	0.98376	0.99410	1.00000
0.821- 0.498	0.16473	0.58862	0.74387	0.84549	0.91607	0.95609	0.97677	0.99171	1.00000
0.498- 0.302	0.12122	0.49596	0.66771	0.78725	0.87424	0.93058	0.96545	0.98850	1.00000
0.302- 0.200	0.09054	0.42435	0.60527	0.73822	0.83941	0.91234	0.96142	0.98887	1.00000

TABLE III

Summary of Neutron Spectrum Measurements

Radius (cm)	Angle (degrees)		
	Fast	Intermediate	Thermal
20.3	0 ± 10.4		0
	30 ± 10	30 ± 10	90
35.6	0 ± 5.9		0
	16.6 ± 6	16.6 ± 6	90
	34.8 ± 6	34.8 ± 6	
	58.9^{+12}_{-9}	58.9^{+12}_{-9}	
50.8	0 ± 3.6		0
	11.5 ± 4	11.5 ± 4	90
	23.6 ± 4.5	23.6 ± 4.5	
	36.9 ± 5	36.9 ± 5	
66.0	0 ± 3.2		

is significant only for the fast-neutron measurements. Channel widths were 0.031 μsec for fast-neutron and 0.125 μsec for intermediate-energy-neutron measurements. The energy resolution, $\Delta E/E = 2\,\Delta t/t$, is thus 2% at 0.8 MeV and increases as $E^{1/2}$ for higher energies. With the boron capture detector, the resolution is 5% at 0.1 MeV and proportional to $E^{1/2}$. The resolution of the thermal-energy measurements is basically determined by the emission time. The mean and variance of the emission time were calculated by the GATHER-II code,[8] checked against the measured dieaway.

[8] G. D. JOANOU, C. V. SMITH, and H. A. VIEWEG, "GATHER-II, An IBM-7090 FORTRAN-II Program for the Computation of Thermal Neutron Spectra and Associated Multigroup Cross Sections," GA-4132, General Atomic (1963).

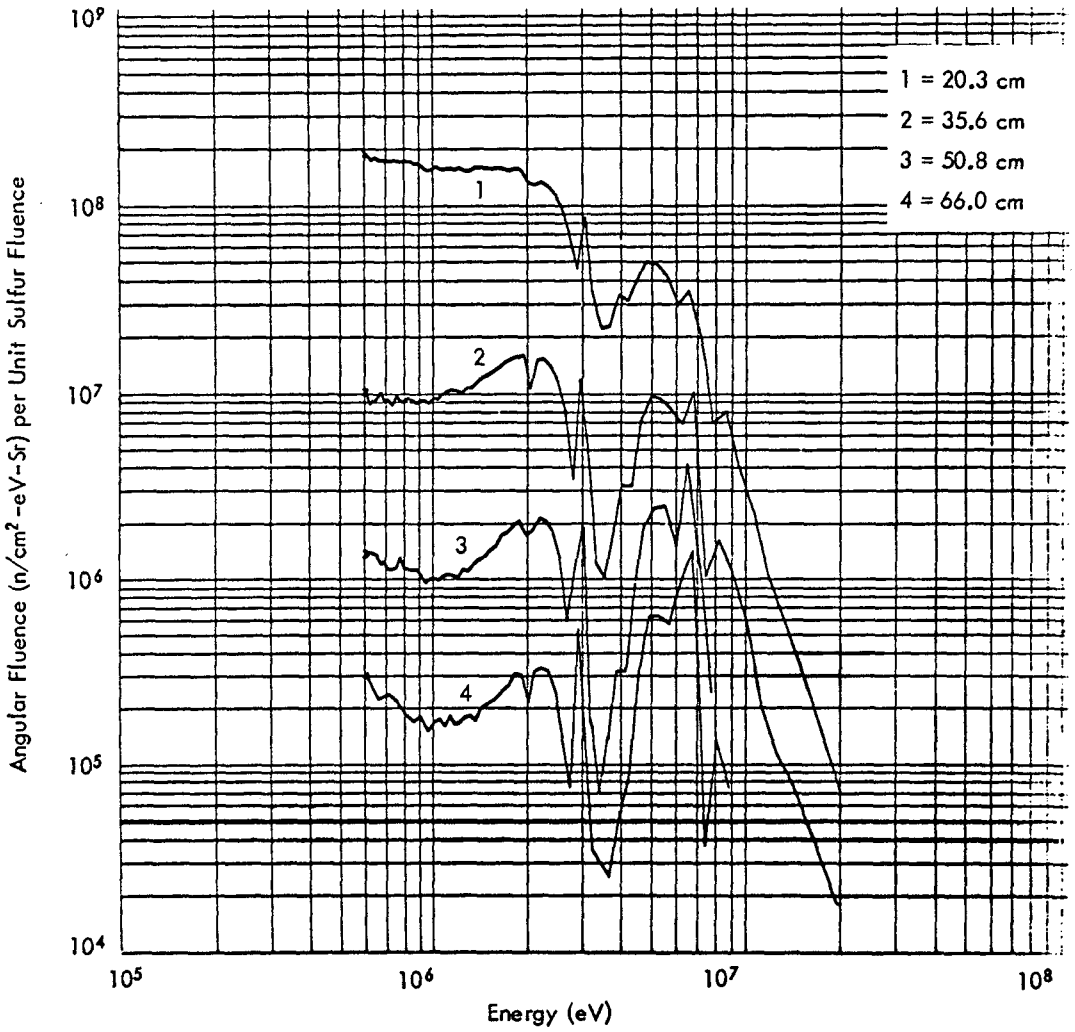

Fig. 4. Fast neutron spectra at 0° vs radius.

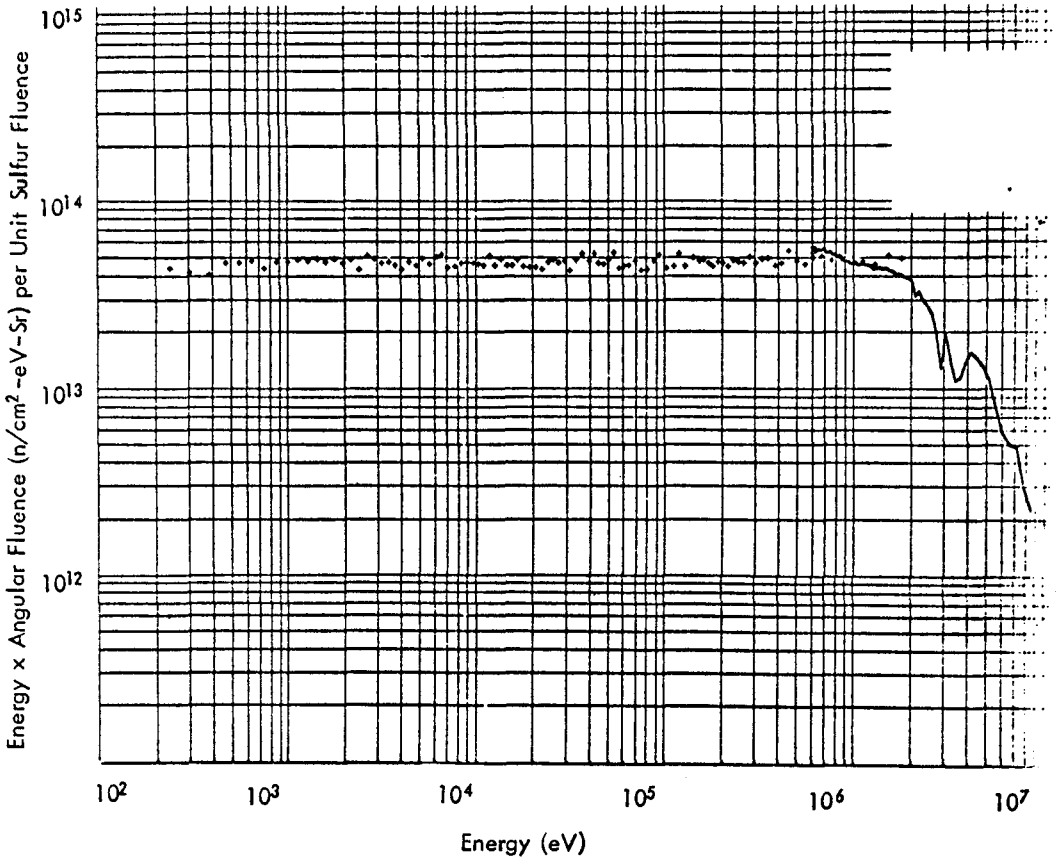

Fig. 5. High-energy spectrum at 20.3 cm and at an angle of 30°.

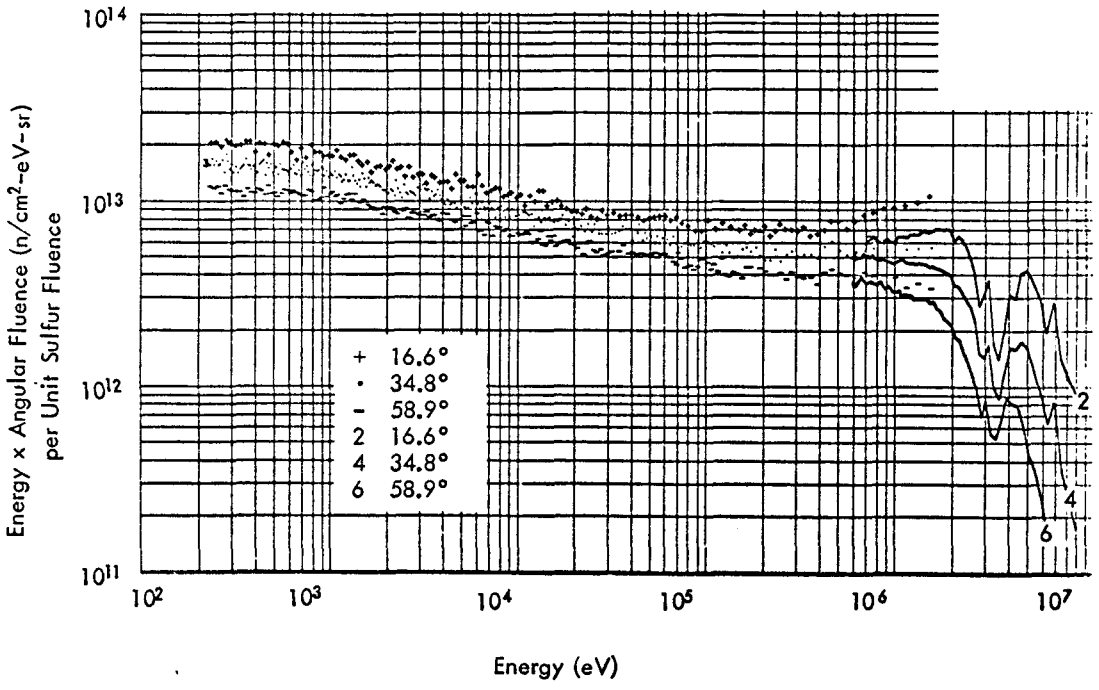

Fig. 6. High-energy spectra at $r = 35.6$ cm.

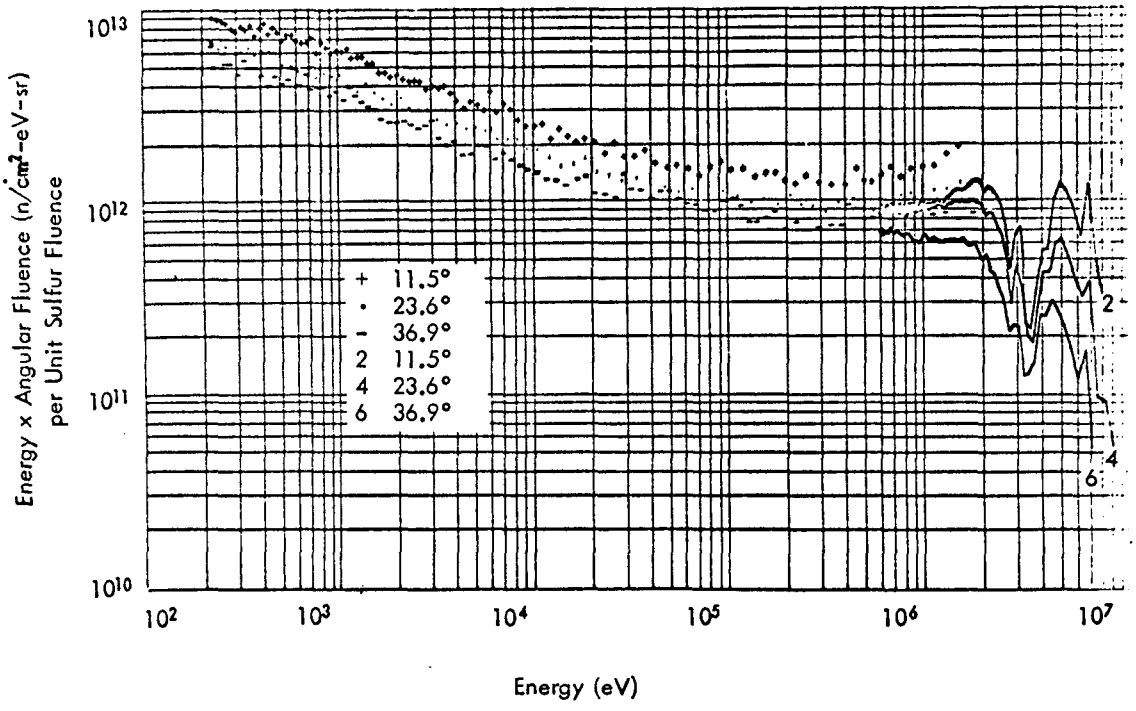

Fig. 7. High-energy spectra at r = 50.8 cm.

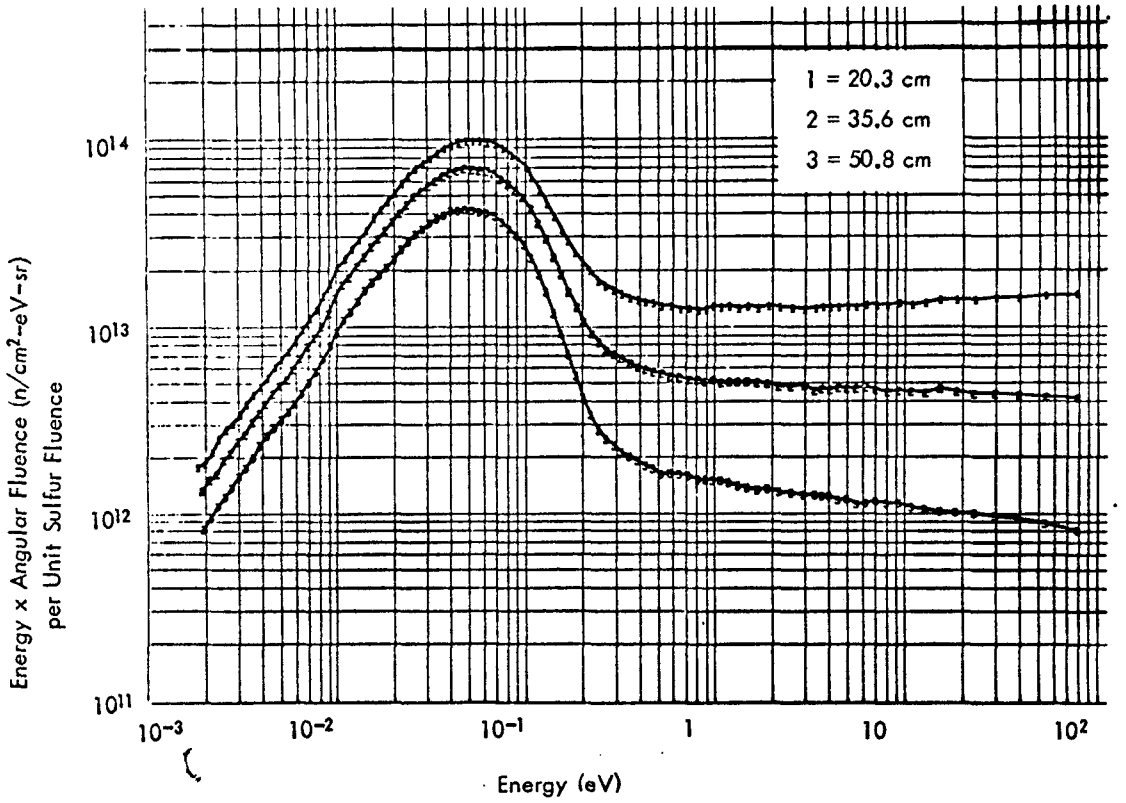

Fig. 8. Low-energy spectra at 0° vs radius.

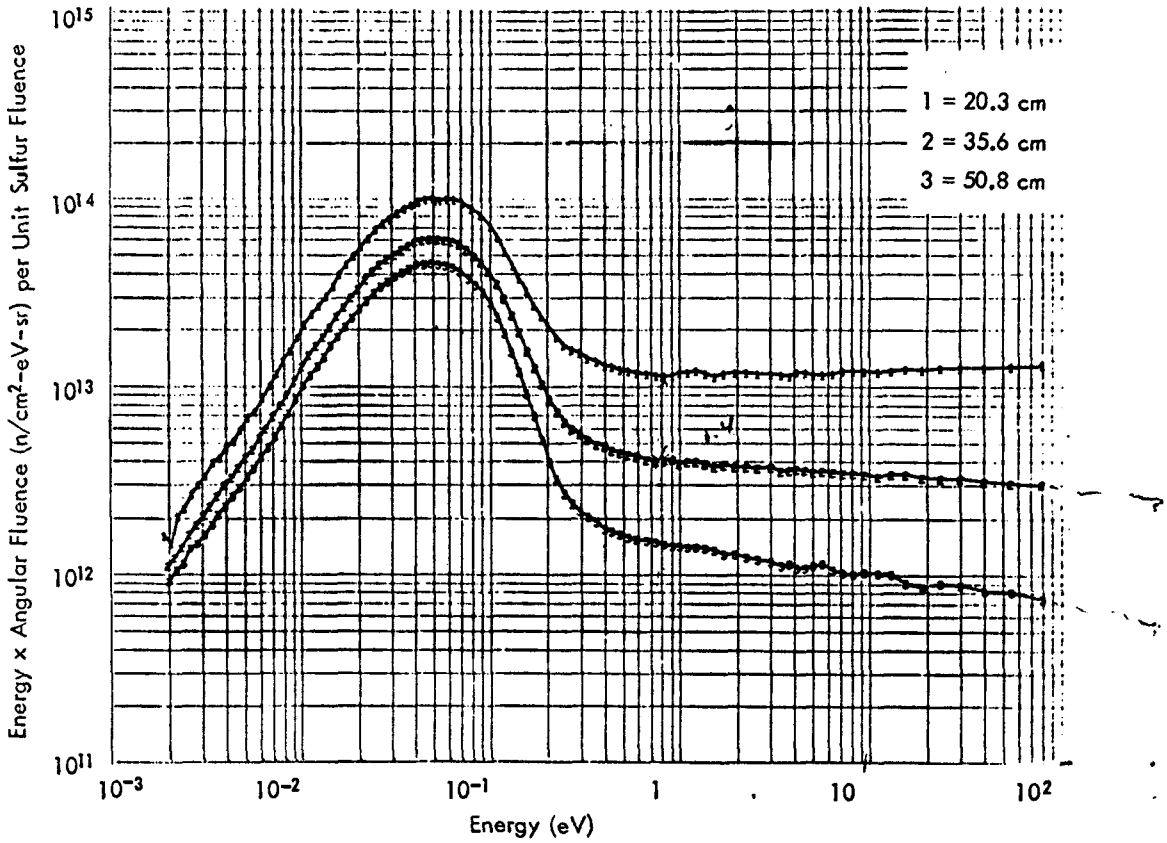

Fig. 9. Low-energy spectra at 90° vs radius.

No correction has been made for resolution. Resolution should be considered in comparing measurements and calculations where the flux is varying rapidly, as in resonances and in the transition region near 0.1 eV.

The error in the flux measurements includes the statistical error in the counts, the errors in the detector efficiency, flight-path transmission, solid angle and viewed area factor, monitor normalization, background subtraction, and perturbations. The statistical error is ± 1 to 5% except for the lowest flux range > 8 to 10 MeV, where channels are grouped to maintain at least ± 10% precision.

The absolute efficiency of the fast-neutron detectors is known to ± 8%, that of the boron capture is known to ± 16%, and the BF_3 bank to ± 7%. The transmission is known to ± 3 to 6% over most of the energy range, but the error may be up to ± 12% between 200 eV and 10 keV with the depleted uranium filter in place. The error in the solid angle and viewed area is estimated at < 5% and affects only the magnitude and not the shape of the spectrum taken with one detector. The monitor normalization is accurate to ~± 3%.

The background in the NE211 and NE213 detectors consists of an exponentially decaying "afterglow" (τ = 0.12 μsec) at short times after the bremsstrahlung burst, followed by a nearly constant component due to ambient activity and other sources of gamma rays. Afterglow is subtracted after extrapolating as $\exp(-t/0.12\ \mu\text{sec})$ from early times where very few counts are due to neutrons. The correction is small below 8 MeV, but there may be an uncertainty ≥ 20% at 10 to 15 MeV in the NE213. The smaller NE211 detector absorbs less bremsstrahlung energy, the fluorescence dieaway is much faster, and little afterglow background is observed. The zero-degree measurements at 20.3- and 35.6-cm radius were made with the NE211 detector.

The constant component of the background in the NE211 and NE213 measurements is found from the average count in the interval 9 to 15 μsec after the burst, corresponding to neutron energies below the bias of the detector. Bremsstrahlung and gamma rays from inelastic scattering arrive at the detector before the neutrons. The thermal capture gamma rays have a time constant of ~2 msec, hence are substantially constant over 15 μsec. Isomeric decay gamma rays from photofission products in the target have half-lives in the measured range, but they are overwhelmed by

buildup of millisecond activities following beta decay at the 360/sec repetition rate. The fission-product activity is detected in zero-degree measurements (viewing the target), but off-zero the background is close to ambient activity. The correction was small in any event, and the contribution to the error in the flux is estimated at ± 1%.

Background for the boron capture detector was found from the average of the counts recorded from 3000 to 3500 μsec after the neutron burst, corresponding to neutron energies below 1.5 eV. The ^{10}B filter in the flight path removed essentially all of the neutrons below 10 eV; hence, the background includes ambient activity and any beam-dependent gamma rays with several millisecond or longer half-lives. It does not include the shorter half-life activities. Since the boron capture detector is much more sensitive to gamma rays than neutrons, the zero-degree measurements are suspect and are not plotted. Near-zero measurements also tend to lie somewhat high compared to the NE213 results in their region of overlap. At larger angles, the uncertainty in the flux due to the background correction is estimated at ± 5% in the 0.1-MeV region, increasing to perhaps ± 25% at energies < 10 keV because of the decreasing signal-to-background ratio.

Background for the BF_3 counter measurements was found in a separate run with a ^{10}B plug located at the bottom of the probe hole in the graphite. The plug absorbs nearly all the low-energy neutrons originating at the point of measurement. The beam-independent (ambient) background was subtracted first and then the beam-dependent background as ratioed by the monitor counts in the data and background runs. The error in the flux due to uncertainty in background subtraction is estimated at <5%.

Possible perturbations in these measurements include the source anisotropy, spurious sources, room return, and the probe-hole perturbation. The anisotropy of the source emission is ± 5% or less, and spurious sources are believed to be negligible. Room return is insignificant for these measurements well inside the stack. The largest effect of the probe hole is expected at large angles (since near 0° the flux is little affected by removal of scatterer beyond the measurement point) and in the intermediate energy range where the 7.62-cm-diam probe hole is up to 3 mfp across. A check measurement at 60° with different size probe holes showed the perturbation was <10%. At higher and lower energies and smaller angles, the perturbation is probably < 5%.

Assuming the errors combine more or less independently, the typical accuracy of the absolute flux is ± 13% for the BF_3 detector measurements, ± 22 to 32% for the boron capture detector, and ± 13 to 23% for the fast-neutron detectors, varying with the energy range as discussed.

IV. CALCULATIONS

The fast-neutron angular flux spectrum measurements have been compared with 05R Monte Carlo code[9] calculations and anisotropic discrete ordinates calculations using the IDF version of the DTF-IV code.[10] Source and inelastic scattering subroutines and a spherical geometry angular flux analysis program were written for use with 05R.

The source in 05R was represented as an outward-directed emitter on a surface of 4.45-cm radius with the spectrum given in Table I and the angular distribution given in Table II. The uranium, water, and stainless steel target materials were omitted for simplicity, hence interactions with backscattered neutrons were not taken into account. Cross sections for carbon were taken from the ENDF/B library, which is based on the Slaggie and Reynolds evaluation.[11] A direct analog Monte Carlo calculation was performed, and the flux crossing the spherical surfaces at 20.3- and 35.6-cm radii was accumulated in appropriate energy and angle bins. The results are shown in Figs. 10 and 11. The measurements have been normalized to the calculations at 20.3 cm and zero degrees.

Agreement between measurement and 05R calculation is reasonably good except near 3.5 MeV. The 0° calculated flux at 35.6 cm is 1.9 times the measured flux averaged over 3.0 to 3.7 MeV and 1.4 times the measured averaged flux from 3.7 to 4.0 MeV. We believe the discrepancy is due to an error in the total cross section for carbon. Slaggie and Reynolds[11] fit optical model calculations to the data of Fossan *et al.*[12] The data of Tsukada and Fuse[12] are in good agreement. The Freier *et al.*[12] data are lower, while the Glasgow and Foster[12] data are ~10% higher. At these high energies, a good estimate of the change in the well-collimated, 0° spectrum with a change in

[9] D. C. IRVING, R. M. FREESTONE, Jr., and F. B. K. KAM, "05R A General Purpose Monte Carlo Neutron Transport Code," ORNL-3622, Oak Ridge National Laboratory (1965).

[10] K. D. LATHROP, "DTF-IV, A FORTRAN-IV Program for Solving the Multigroup Transport Equation with Anisotropic Scattering," LA-3373, Los Alamos Scientific Laboratory (1965).

[11] E. L. SLAGGIE and J. T. REYNOLDS, "C^{12} Fast Neutron Cross Sections and Legendre Moments Below 15.0 MeV," KAPL-3099, Knolls Atomic Power Laboratory (1966).

[12] BNL-325, 2nd ed., Supp. 2, Vol. 1, Brookhaven National Laboratory (1964).

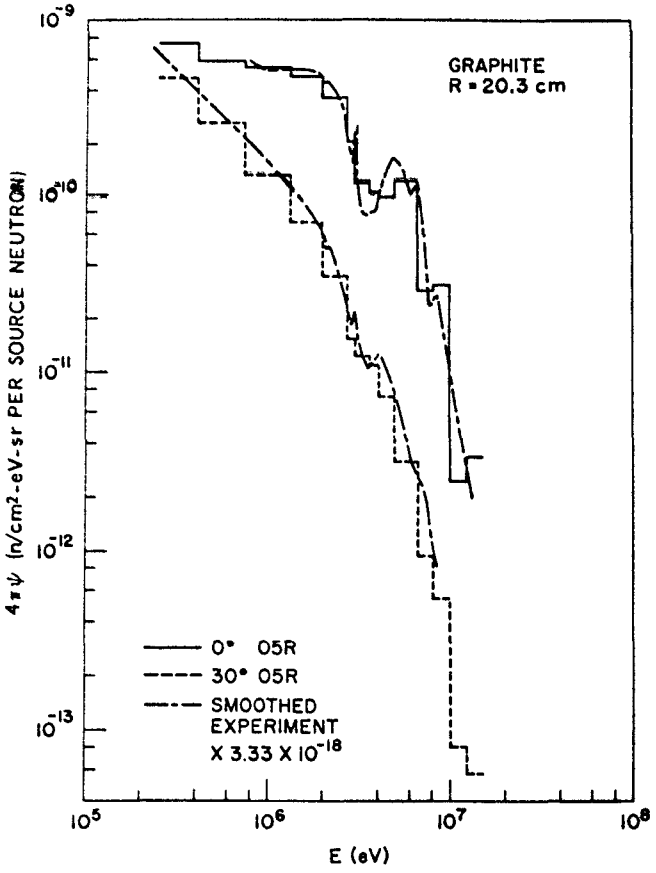

Fig. 10. Comparison of 05R and measured spectra at 20.3 cm.

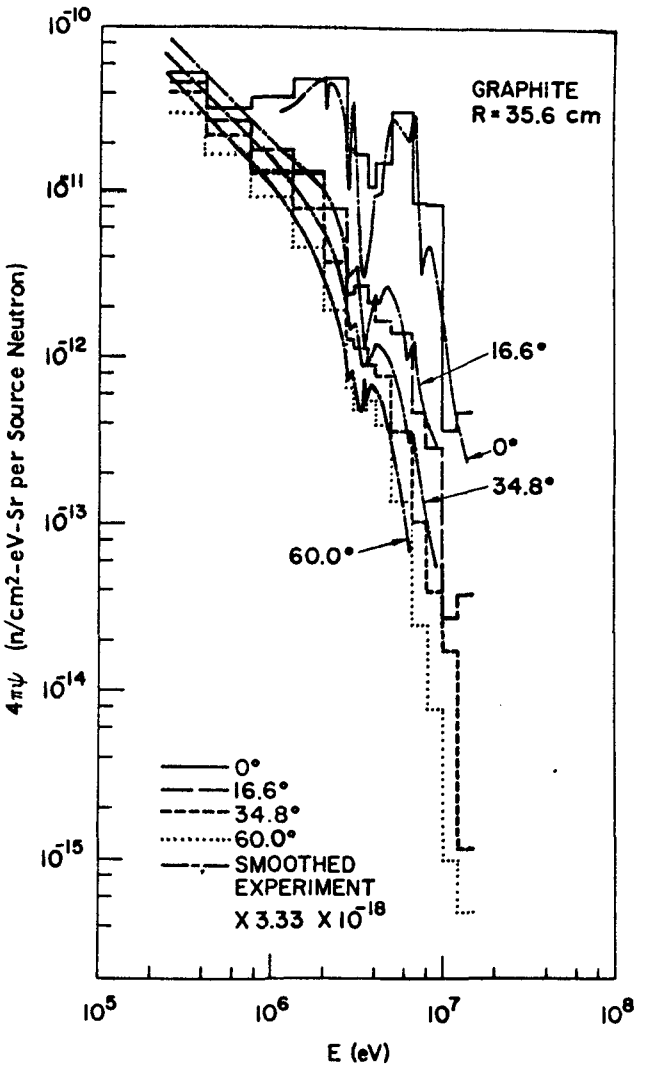

Fig. 11. Comparison of 05R and measured spectra at 35.6 cm.

σ_T can be obtained from a simple exponential attenuation calculation. Such a calculation shows that a 10% increase in the total cross section near 3.5 MeV will give much better agreement with the spectrum measurement. Later measurements by Yergin *et al.*[13] also indicate that the total cross section is larger than in ENDF/B. It is interesting to note the sensitivity of the 0° spectrum to a small error in the cross section.

The 1DF calculations were performed with 15-group P_3 cross sections (0.1 to 14.9 MeV) obtained from an infinite-medium B_3 calculation in the GAM-II code[14] using ENDF/B data. The calculation was made in spherical geometry with an outer radius of 80 cm, and the spherical, water-cooled, depleted uranium target was included explicitly. The source was a uniform isotropic emitter in a 0.85-cm-radius volume imbedded at the center of the uranium, with a photoneutron spectrum which gave agreement with the measured target leakage spectrum. The 1DF calculated and measured angular flux spectra are compared in Fig. 12. The measurements are normalized to the calculations at 60 to 62.7° and 1 to 2 MeV. Agreement is rather good except in resonances where the energy resolution in the calculation is too coarse to reproduce the experimental detail. The angular resolution in the calculation is poorer than the experimental resolution, and a much finer angular mesh is required to calculate the angular distribution near zero degrees.

The scalar flux spectrum has been calculated by moments, 1DF, and 05R, all using the basic ENDF/B data. The moments calculation was per-

[13]P. F. YERGIN et al., "MeV Total Cross Sections with the Rensselaer LINAC," *Proc. Conf. Neutron Cross Section Technology, Washington, D.C., March 22-24, 1966*, CONF-660303,

[14]G. D. JOANOU and J. S. DUDEK, "GAM-II, A B_3 Code for the Calculation of Fast Neutron Spectra and Associated Multigroup Constants," GA-4265, General Atomic (1963).

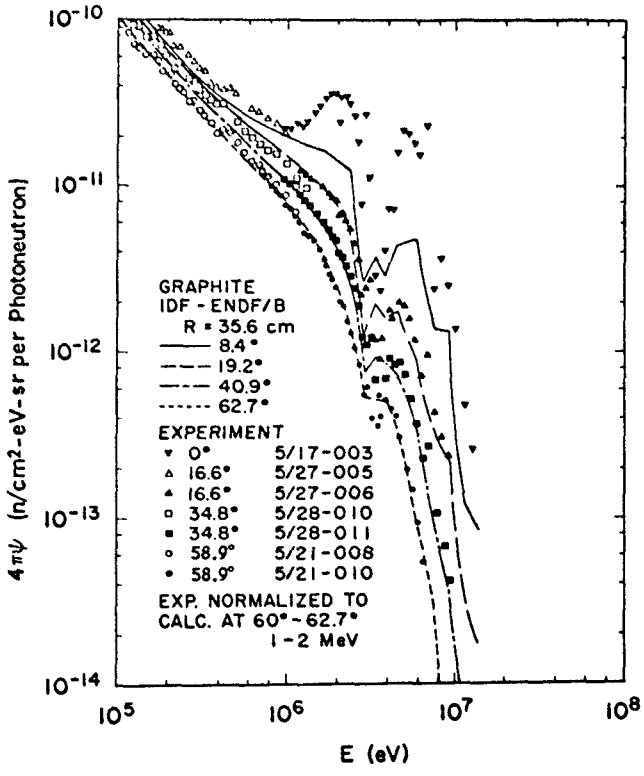

Fig. 12. Comparison of 35.6-cm measurements and 1DF-ENDF/B calculation.

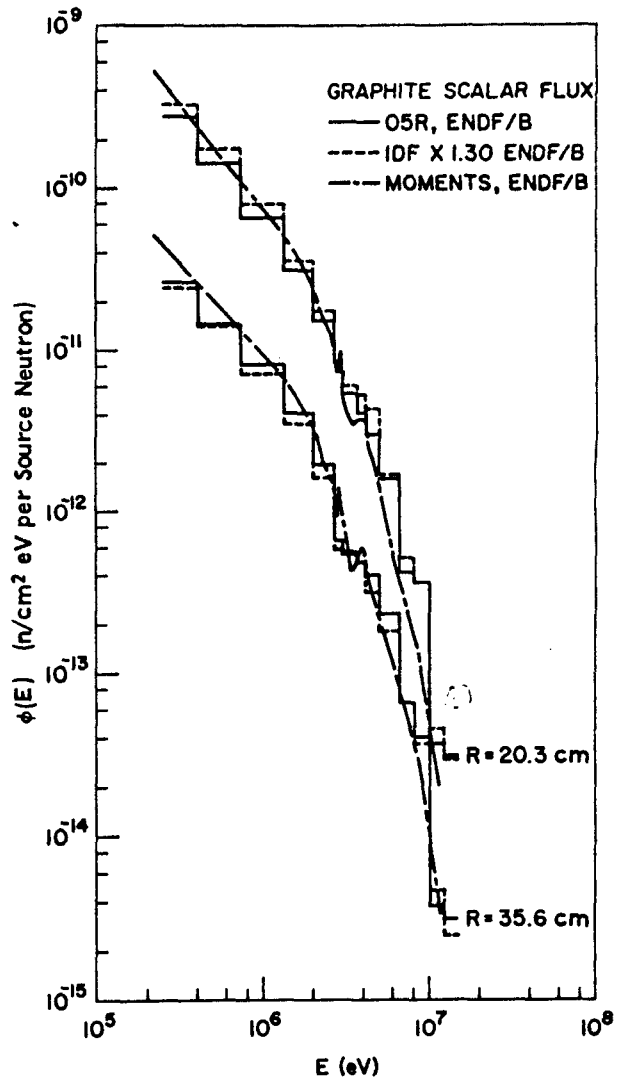

Fig. 13. Calculated scalar fluxes in graphite.

formed by Eisenhauer[15] and will be published later. The source was assumed to be point isotropic imbedded in infinite graphite. The spectrum was essentially that in Table I. The quantity $N = 4\pi r^2 \phi(E)$ was calculated for $\mu_0 r = 1, 2, 3, 4, 5$, where μ_0 is the macroscopic total cross section at 15 MeV. These were interpolated as ln N vs $\mu_0 r$ at r minus 4.45 cm and divided by $4\pi r^2$ to give the scalar flux at $r = 20.3$ and 35.6 cm in graphite at a density of 1.64 g/cm^3. The spectrum is plotted in Fig. 13 along with the 05R and 1DF results. The 1DF calculations for one photoneutron per sec have been multiplied by 1.30 to convert to one target leakage neutron per sec. This value is subject to some revision as improved target calculations with fissioning included are made.

The moments calculation was made with a finer energy mesh than 1DF, and there is more detail in the resonance region. Part of the discrepancy in the average flux may be due to the differences in the source, although, in our experience, the scalar flux is not very sensitive to the angular distribution of the source emission. This example illustrates one of the problems in testing codes by comparing one calculation with another: it is difficult to make them identical in every respect except for the method used to solve the transport equation. We do not have scalar flux spectrum measurements in graphite to test the moments calculations directly, and angular distributions could not be obtained from moments for lack of suitable fitting functions. The 05R calculated scalar flux is probably the best for comparison and is given in Table IV.

V. CONCLUSIONS

High-resolution measurements of the neutron angular flux in graphite have provided a good test of the nuclear data for graphite and of the ability of theoretically rigorous codes to calculate the

[15] C. EISENHAUER and L. V. SPENCER, "Neutron Flux from a Point Isotropic Source in Carbon Calculated by the Moments Method," to appear as a National Bureau of Standards Report.

TABLE IV

O5R Calculated Scalar Flux

E(eV)		$\varphi(E)$ n/cm^2 eV per Source Neutron	
		R = 20.3 cm	R = 35.6 cm
2.47 + 5 to	4.08 + 5	2.789 - 10	2.652 - 11
4.08 + 5	7.43 + 5	1.459 - 10	1.443 - 11
7.43 + 5	1.35 + 6	6.583 - 11	8.202 - 12
1.35 + 6	2.02 + 6	3.114 - 11	4.066 - 12
2.02 + 6	2.73 + 6	1.534 - 11	1.993 - 12
2.73 + 6	3.01 + 6	7.321 - 12	6.700 - 13
3.01 + 6	3.68 + 6	5.382 - 12	5.653 - 13
3.68 + 6	4.07 + 6	4.056 - 12	4.909 - 13
4.07 + 6	4.97 + 6	3.022 - 12	3.998 - 13
4.97 + 6	6.70 + 6	1.620 - 12	2.334 - 13
6.70 + 6	8.19 + 6	4.184 - 13	6.610 - 14
8.19 + 6	1.00 + 7	3.646 - 13	4.061 - 14
1.00 + 7	1.22 + 7	3.700 - 14	3.740 - 15
1.22 + 7	1.49 + 7	3.115 - 14	3.168 - 15

angular and energy distributions. The discrepancy between the measured and calculated spectrum at 0° indicates the total cross section for carbon in the ENDF/B library is too low by ~10% in the 3.5-MeV resonance. Otherwise, the 05R Monte Carlo code with our source, inelastic scattering, and analysis programs gave excellent agreement with experiment.

The 1DF discrete ordinates code gave fairly good agreement off 0°, but the energy group structure was too coarse to reveal all the detail in the measurement. The ENDF/B cross sections, averaged in GAM-II and truncated at P_3, and the Gauss-Legendre n = 16 angular quadrature were adequate except at 0°, where a finer angular mesh is needed to match the experimental resolution. Previous experience had indicated that P_1 scattering was not adequate for calculation of fast-neutron penetration.

The moments calculations were performed by Eisenhauer,[15] using the ENDF/B cross sections. Agreement with the 05R calculated scalar flux is not as good as might be expected, perhaps because of the difference in source representation.

Low-energy calculations were not performed but the experimental data are available for those who wish to make a theory-experiment comparison. Leakage must be taken into account for the thermal neutrons because of the low-absorption cross section of the graphite.

ACKNOWLEDGMENTS

We are grateful to Charles Eisenhauer for permission to quote his moments calculation results. Professor T. G. Williamson participated in part of the experimental program. We also acknowledge the help of members of the Accelerator Physics staff, including J. R. Beyster, J. L. Russell, Jr., J. H. Audas, W. Brouwer, G. P. Demers, G. K. Houghton, and G. E. Rogers.

This work was supported by the Defense Atomic Support Agency under Contract DA-49-146-XZ-482.